Path planning of hyper-redundant manipulator in developed view

Lukáš Bláha
Department of cybernetics
University of West Bohemia
Pilsen, Czech Republic
frere@kky.zcu.cz

Martin Švejda
Department of cybernetics
University of West Bohemia
Pilsen, Czech Republic
msvejda@kky.zcu.cz

***Abstract*—The paper deals with the path planning of hyper-redundant manipulator as a part of NDT technology for circumferential welds on pipe with limited accessibility. Ability to move along the tested weld in very confined space is the major feature which is considered for NDT inspections. Documentation of such a weld and nearby environment typically contains a drawing with Developed view. Such a drawing is beneficially used as a basic input for path planner. The redundant degrees of freedom of manipulator are then used for optimization the robot body shape. The method for intuitive path planning in constrained environment was developed. It is based on obstacle definition via attractive and repulsive objects described in Developed view together with weighted least norm algorithm for robot body fitting around the pipe regarding obstacle avoidance. The proposed planning method and fitting algorithm were tested and proved via virtual robot model with 13 degrees of freedom.**

***Keywords*—path planning, NDT inspection, Developed view, hyper-redundant manipulator, optimal algorithm**

I. Introduction

Recent progress in robotic related fields brings new opportunities in development of serial hyper-redundant mechanisms or snake-like robots [1] used for teleoperated or fully automated visual inspections [2]. Methods for path planning and robot fitting along the path are of great importance too [3]. The key point for robotic manipulators analysis and control is the capability to transform the task space coordinates into the joint space [4]. For hyper-redundant manipulators the problem is much more apparent because there exists infinitely many solutions of inverse kinematics [5]. Nevertheless robotic manipulators with additional degrees of freedom (DOF) are preferable in many complex applications and tasks. Kinematical redundancy aims to offer greater flexibility and dexterity in the motion of manipulator. As there are infinitely many solutions for the inverse kinematics, many issues related to some constraints, for example joint limits, can be contained in the control-law design [5]. Therefore effective utilization of redundancy is the hot topic in the path planning and control of the redundant manipulators.

The motivation to this research arises from demand to inspect and estimate the degradation and lifespan of pipeline welds, mostly tested in power plants, using some autonomous or semi-autonomous device or robot. Nondestructive methods (NDT) are of greatest importance as they allow systematic monitoring of industrial components that are fully integrated in the technology without the necessity to substitute them after each inspection. The standard tasks and methods for NDT weld inspection are described in [2]. Ability to move around the testing component in very confined space is the major feature which has to be considered for NDT inspections. Nowadays, the majority of inspections are performed via hand device, as depicted in the following figure, and the problem is that measuring accuracy and repeatability is rather poor. Therefore there is a growing demand for robotic device to overlap these issues, especially to solve the problems with NDT inspections in constrained environments.

Fig. 1. Typical NDT setting for manual weld inspection.

II. Manipulator Kinematics

Hyper-redundant robots are most commonly built as a serial chains of rigid links connected by rotational joints. Shape of these robots, and thus the primary control space, is specified by the vector of joint angles and several good algorithms have appeared in the literature for body fitting to the prescribed curve [1]. The structure of proposed NDT manipulator consists of circumferential carriage module with 1DOF followed by 6DOF serial manipulator, ended by 6DOF lightweight robot arm with special joint [8]. This assembly arises from NDT

978-1-5386-4762-2/18/$31.00 ©2018 IEEE

inspection demands, functional and feasibility restrictions. Note that the following techniques are not limited by number of DOF.

The whole kinematics can be described by the Denavit Hartenberg convention [9], see Fig. 2. D-H parameters are summarized in Table I.

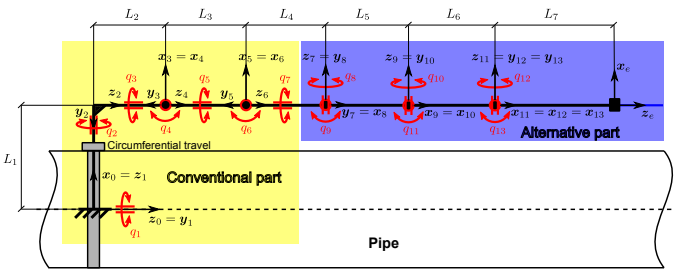

Fig. 2. Coordinate systems of manipulator according to D-H convention.

i	d_i	θ_i	a_i	α_i
1	0	θ_1	0	$\frac{\pi}{2}$
2	L_1	θ_2	0	$-\frac{\pi}{2}$
3	L_2	θ_3	0	$-\frac{\pi}{2}$
4	0	θ_4	0	$\frac{\pi}{2}$
5	L_3	θ_5	0	$-\frac{\pi}{2}$
6	0	θ_6	0	$\frac{\pi}{2}$
7	L_4	θ_7	0	$\frac{\pi}{2}$
8	0	θ_8	0	$\frac{\pi}{2}$
9	0	θ_9	L_5	$-\frac{\pi}{2}$
10	0	θ_{10}	0	$\frac{\pi}{2}$
11	0	θ_{11}	L_6	$-\frac{\pi}{2}$
12	0	θ_{12}	0	$\frac{\pi}{2}$
13	0	θ_{13}	0	0

TABLE I
D-H PARAMETERS OF MANIPULATOR

Joints coordinates are defined as:

$$\boldsymbol{Q} = \begin{bmatrix} \theta_1 & \theta_2 & \dots & \theta_{12} & \theta_{13} \end{bmatrix}^T \tag{1}$$

The end-effector coordinates are defined as a 3x4 matrix composed of translation vector and rotation matrix:

$$\boldsymbol{X}_{full} = \begin{bmatrix} \boldsymbol{O}_e^0 & \boldsymbol{R}_e^0 \end{bmatrix} = \begin{bmatrix} O_x & x_x & y_x & z_x \\ O_y & x_y & y_y & z_y \\ O_z & x_z & y_z & z_z \end{bmatrix}$$

Kinematic parameters are defined as the manipulator links lengths and the end-effector compensation - translation vector and rotation matrix:

$$\boldsymbol{\xi} = \begin{bmatrix} L_1 \\ L_2 \\ \vdots \\ L_7 \end{bmatrix}, \quad \boldsymbol{T}_e^{13} = \begin{bmatrix} 0 & 0 & 1 & L_7 \\ 1 & 0 & 0 & 0 \\ 0 & 1 & 0 & 0 \\ 0 & 0 & 0 & 1 \end{bmatrix} \tag{2}$$

Forward kinematic model

The standard forward kinematics model is implemented as follows:

$$\begin{aligned} \boldsymbol{O}_e^0 &= \boldsymbol{T}_e^0[1:3,4], \quad \boldsymbol{R}_e^0 = \boldsymbol{T}_e^0[1:3,1:3] \\ \boldsymbol{T}_e^0 &= \prod_{i=1}^{13} \boldsymbol{T}_i^{i-1}(d_i, \theta_i, a_i, \alpha_i) \cdot \boldsymbol{T}_e^{13} \end{aligned} \tag{3}$$

where:

$$\boldsymbol{T}_i^{i-1} = \begin{bmatrix} \cos\theta_i & -\sin\theta_i \cos\alpha_i & \sin\theta_i \sin\alpha_i & a_i \cos\theta_i \\ \sin\theta_i & \cos\theta_i \cos\alpha_i & -\cos\theta_i \sin\alpha_i & a_i \sin\theta_i \\ 0 & \sin\alpha_i & \cos\alpha_i & d_i \\ 0 & 0 & 0 & 1 \end{bmatrix}$$

Then the standard forward instantaneous kinematics for velocities and accelerations is given as:

$$\begin{aligned} \begin{bmatrix} \dot{\boldsymbol{O}}_e^0 \\ \boldsymbol{\omega}_e^0 \end{bmatrix} &= \boldsymbol{J}_e^0(\boldsymbol{Q}) \cdot \dot{\boldsymbol{Q}}, \\ \begin{bmatrix} \ddot{\boldsymbol{O}}_e^0 \\ \dot{\boldsymbol{\omega}}_e^0 \end{bmatrix} &= \dot{\boldsymbol{J}}_e^0(\boldsymbol{Q}, \boldsymbol{Q}) \cdot \dot{\boldsymbol{Q}} + \boldsymbol{J}_e^0(\boldsymbol{Q}) \cdot \ddot{\boldsymbol{Q}} \\ \dot{\boldsymbol{R}}_e^0 &= \boldsymbol{S}(\boldsymbol{\omega}_e^0) \cdot \boldsymbol{R}_e^0 \end{aligned} \tag{4}$$

where $\boldsymbol{J}_e^0(\boldsymbol{Q})$ resp. $\dot{\boldsymbol{J}}_e^0(\dot{\boldsymbol{Q}}, \boldsymbol{Q})$ is the kinematic jacobian resp. its time derivative, $\boldsymbol{S}(\star)$ is a skew-symmetric matrix and $\boldsymbol{\omega}_e^0$ is angular velocity of end effector with respect to inertial frame.

III. Developed View

The basic part of path planning is to think about the task space of given hyper-redundant manipulator. Fig. 3 reflects the typical situation of circumferential weld on pipe with limited accessibility. Documentation of such a weld and nearby environment typically contains a drawing with so-called Developed view, see Fig. 4. Such a drawing is assumed to be a basic input for operator command control. Therefore, it seems to be useful to restrict the path planning to a plane, which originates from pipe Developed view. The elevation above the pipe is additional parameter for path planner.

Instead of standard 6DOF end-effector representation (3, 4) the new end-effector coordinates are introduced and called as DV coordinates. The coordinates project the standard 6DOF end-effector coordinates on pipe surface (analogously as cylindrical coordinates transformation). In this Developed view only four coordinates are defined and controlled because the remaining DOF are covered by passive NDT probe holder which ensures pipe surface contact with an additional 1DOF rotation for probe heading. The probe holder including its active heading is not further discussed.

The proposed DV coordinates

$$\bar{\boldsymbol{X}} = \begin{bmatrix} l & z & h & \alpha \end{bmatrix}^T \tag{5}$$

define the position of entire holder where l is the pipe perimeter, z is the length of pipe, h is the height above pipe

surface and α is the last manipulator link orientation projected onto the pipe surface.

Fig. 5 shows the typical setting and Developed view of pipe with two perpendicular tube inlets as a typical kind of obstacles which has to be avoided during the testing process together with weld, manipulator and railway.

Fig. 3. Photo-documentation of circumferential weld on a pipe with limited accessibility.

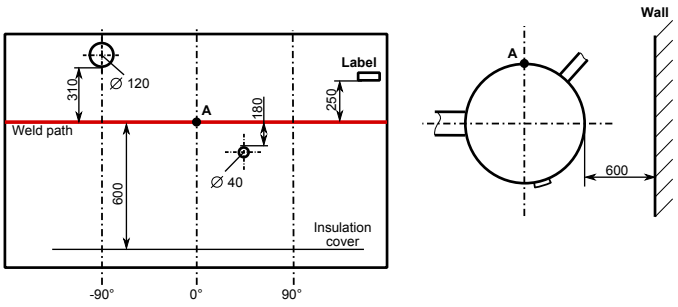

Fig. 4. Typical drawing of pipe weld using the Developed view.

The transformation from end-effector coordinates $\boldsymbol{X}$ (only translation $\boldsymbol{O}_e^0$ and the axis $\boldsymbol{z}_e^0$ - projection of the last link on the pipe surface $\Rightarrow$ orientation α) to DV coordinates $\bar{\boldsymbol{X}}$ is given as:

$$\boldsymbol{X} = \begin{bmatrix} O_x & O_y & O_z & z_x & z_y & z_z \end{bmatrix}^T \text{ (standard gen. coords.)}$$
$$\bar{\boldsymbol{X}} = \begin{bmatrix} l & z & h & \alpha \end{bmatrix}^T \text{ (new DV coords.)}$$

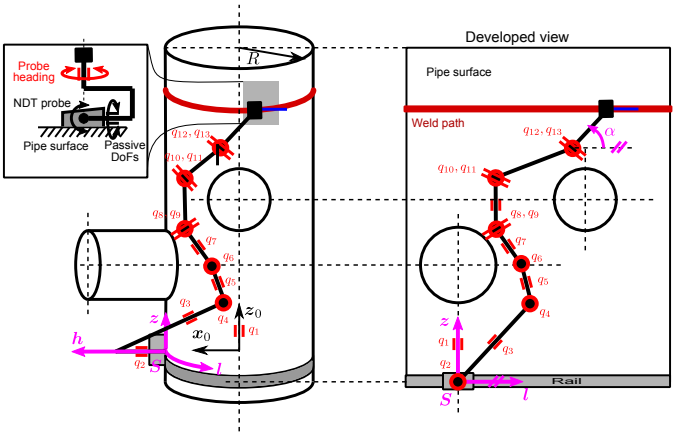

Fig. 5. Hyper-redundant manipulator setting on pipe surface and in Developed view.

$$\bar{\boldsymbol{X}} = \mathbf{F}(\boldsymbol{X}) = \begin{bmatrix} \arctan(O_y, O_x)\, R \\ O_z \\ -\frac{\sqrt{(O_y{}^2 + O_x{}^2)^{-1}} R - 1}{\sqrt{(O_y{}^2 + O_x{}^2)^{-1}}} \\ \arctan\left(z_z, \frac{O_x\, z_y}{\sqrt{O_y{}^2 + O_x{}^2}} - \frac{O_y\, z_x}{\sqrt{O_y{}^2 + O_x{}^2}} \right) \end{bmatrix} \tag{6}$$

where R is the pipe radius.

The transformation between corresponding velocities of the standard and DV coordinates can be expressed by the gradient $\frac{\partial \mathbf{F}(\boldsymbol{X})}{\partial \boldsymbol{X}}$:

$$\dot{\bar{\boldsymbol{X}}} = \frac{\partial \mathbf{F}(\boldsymbol{X})}{\partial \boldsymbol{X}} \cdot \dot{\boldsymbol{X}} \tag{7}$$

And the forward instantaneous kinematic leads to:

$$\dot{\bar{\boldsymbol{X}}} = \bar{\boldsymbol{J}}(\boldsymbol{Q}) \cdot \dot{\boldsymbol{Q}} \tag{8}$$

where:

$$\bar{\boldsymbol{J}}(\boldsymbol{Q}) = \frac{\partial \mathbf{F}(\boldsymbol{X})}{\partial \boldsymbol{X}} \cdot \begin{bmatrix} \boldsymbol{I} & \boldsymbol{O} \\ \boldsymbol{O} & -\boldsymbol{S}(\boldsymbol{z}_e^0) \end{bmatrix} \cdot \boldsymbol{J}_e^0(\boldsymbol{Q})$$
$$\boldsymbol{S}(\boldsymbol{z}_e^0) = \begin{bmatrix} 0 & -z_z & z_y \\ z_z & 0 & -z_x \\ -z_y & z_x & 0 \end{bmatrix}$$

is the jacobian of the manipulator with respect to the DV coordinates $\bar{\boldsymbol{X}}$.

IV. Path Planning

Path planning is used during the ultrasonic testing process, where the manipulator has to avoid the obstacles or go through a confined space toward the weld path to continue weld inspection task. Although the standard path planning methods deal with the problem of precise body fitting to a prescribed curve, inspection task defines two main restrictions. First, the NDT probe has to follow the weld path as precisely as possible. Second, the robot has to be mounted on circumferential rail,

which can be placed often only behind the obstacles. Therefore, a path planning method for NDT inspections, based on obstacle interpretation and collision avoidance in Developed view, has been proposed.

Planning algorithm

This section deals with the strategy of manipulator path planning process, which ensure the precise positioning of NDT probe along the tested weld together with collision avoidance of whole manipulator and surroundings.

After redefinition of forward kinematic problem from previous section (13 joint coordinates and only 4 DV coordinates) it is clear that the proposed manipulator has 9DOF redundancy. Therefore a numerical algorithm for inverse kinematic computation can be used and the redundancy is used for internal manipulator motion optimization which is based on suitable objective function $w(\boldsymbol{Q})$. The objective function evaluates the distance among manipulator links and the obstacles, see Fig. 6, and it is defined as follows:

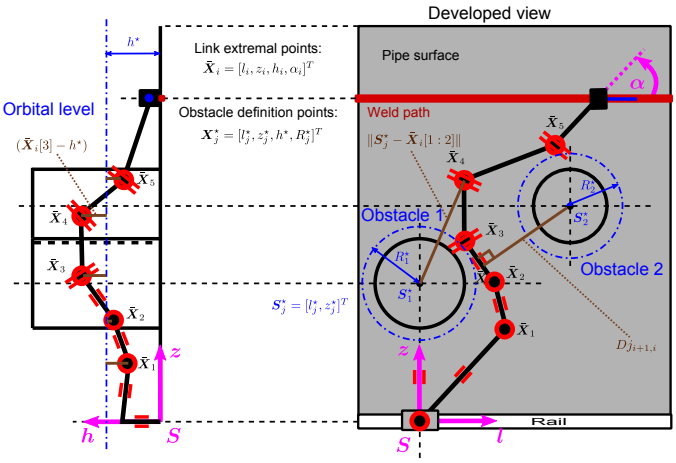

Fig. 6. Representation of objective function in Developed view.

The manipulator link extremal points are defined as follows:

$$\bar{\boldsymbol{X}}_i = \mathbf{F}(\boldsymbol{X}_k), \quad \boldsymbol{X}_k = \begin{bmatrix} \boldsymbol{O}_k^0 \\ \boldsymbol{z}_k^0 \end{bmatrix} = \begin{bmatrix} \boldsymbol{T}_k^0[1:3,4] \\ \boldsymbol{T}_k^0[1:3,3] \end{bmatrix} \tag{9}$$

$$i = \{1,2,3,4\}, \; k = \{4,6,8,10,13\}$$

where $\boldsymbol{T}_k^0$ are homogeneous transformation matrices from the forward kinematics computation (3).

The objective function $w(\boldsymbol{Q})$ consists of the following parts ${}^1w$, ${}^2w_j$, ${}^3w_j$:

1) takes into account the elevation distance of manipulator extremal points $\bar{\boldsymbol{X}}_i = [h_i]$ from pipe surface $h^\star \Rightarrow {}^1w(\boldsymbol{Q})$

$${}^1w(\boldsymbol{Q}) = -\sum_{i=1}^{5} \frac{1}{2} \cdot k_i^2 \cdot (\bar{\boldsymbol{X}}_i - h^\star)^2 \tag{10}$$

$$\frac{\partial {}^1w(\boldsymbol{Q})}{\partial \boldsymbol{Q}} = -\sum_{i=1}^{5} k_i^2 \cdot (\bar{\boldsymbol{X}}_i - h^\star) \cdot \frac{\partial \bar{\boldsymbol{X}}_i}{\partial \boldsymbol{Q}} \tag{11}$$

2) takes into account the distance of manipulator extremal points $\bar{\boldsymbol{X}}_i = [l_i, z_i]^T$ from the center $\boldsymbol{S}_j^\star = [l_j^\star, z_j^\star]^T$ of the j-th circular obstacle with radius $R_j^\star \Rightarrow {}^2w_j(\boldsymbol{Q})$.

$${}^2w_j(\boldsymbol{Q}) = \sum_{i=1}^{5} \frac{1}{2} \cdot w_j^\star \cdot \hat{k}_i \cdot (\|\boldsymbol{S}_j^\star - \bar{\boldsymbol{X}}_i\|^2 - (R_j^\star)^2) \tag{12}$$

$$\hat{k}_i = \begin{cases} k_i^1 & \text{for: } (\|\boldsymbol{S}_j^\star - \bar{\boldsymbol{X}}_i\|^2 - (R_j^\star)^2) < 0 \\ 0 & \text{otherwise} \end{cases}$$

$$\frac{\partial^2 w_j(\boldsymbol{Q})}{\partial \boldsymbol{Q}} = -\sum_{i=1}^{5} w_j^\star \cdot (\boldsymbol{S}_j^\star - \bar{\boldsymbol{X}}_i)^T \cdot \frac{\partial \bar{\boldsymbol{X}}_i}{\partial \boldsymbol{Q}} \tag{13}$$

3) takes into account the distance of manipulator body link $[\bar{\boldsymbol{X}}_i = [l_{i+1}, z_{i+1}]^T, \bar{\boldsymbol{X}}_{i+1} = [l_i, z_i]^T]$ from the center $\boldsymbol{S}_j^\star = [l_j^\star, z_j^\star]^T$ of the j-th circular obstacle with radius $R_j^\star \Rightarrow {}^3w_j(\boldsymbol{Q})$, see Fig. 7.

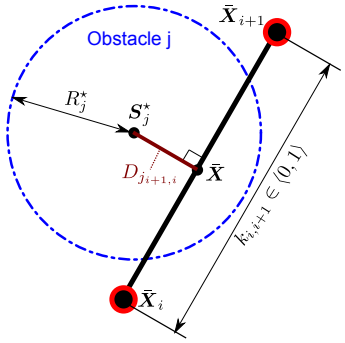

Fig. 7. Manipulator link distance from circular obstacle

$${}^3w_j(\boldsymbol{Q}) = \sum_{i=1}^{4} \frac{1}{2} \cdot w_j^\star \cdot \hat{k}_i \cdot (Dj_{i+1,i}^2(\boldsymbol{Q}) - (R_j^\star)^2) \tag{14}$$

$$\hat{k}_i = \begin{cases} k_i^1 & \text{for: } (Dj_{i+1,i}^2(\boldsymbol{Q}) - (R_j^\star)^2) < 0 \wedge \\ & \quad k_{i,i+1} \in \langle 0,1 \rangle \\ 0 & \text{otherwise} \end{cases}$$

$$\frac{\partial {}^3w_j(\boldsymbol{Q})}{\partial \boldsymbol{Q}} = \sum_{i=1}^{4} w_j^\star \cdot \hat{k}_i \cdot Dj_{i+1,i}(\boldsymbol{Q}) \cdot \frac{\partial Dj_{i+1,i}(\boldsymbol{Q})}{\partial \boldsymbol{Q}} \tag{15}$$

where

$$k_{i,i+1} = \frac{(\boldsymbol{S}_j^\star - \bar{\boldsymbol{X}}_i)^T \cdot (\bar{\boldsymbol{X}}_{i+1} - \bar{\boldsymbol{X}}_i)}{\|\bar{\boldsymbol{X}}_{i+1} - \bar{\boldsymbol{X}}_i\|^2}$$

$$\bar{\boldsymbol{X}} = \bar{\boldsymbol{X}}_i + k_{i,i+1} \cdot (\bar{\boldsymbol{X}}_{i+1} - \bar{\boldsymbol{X}}_i)$$

$$Dj_{i+1,i}(\boldsymbol{Q}) = \left[(\boldsymbol{S}_j^\star - \bar{\boldsymbol{X}})^T \cdot (\boldsymbol{S}_j^\star - \bar{\boldsymbol{X}}) \right]^{\frac{1}{2}}$$

$$\frac{\partial Dj_{i+1,i}(\boldsymbol{Q})}{d\boldsymbol{Q}} = -\left[(\boldsymbol{S}_j^\star - \bar{\boldsymbol{X}})^T \cdot (\boldsymbol{S}_j^\star - \bar{\boldsymbol{X}}) \right]^{-\frac{1}{2}} \cdot (\boldsymbol{S}_j^\star - \bar{\boldsymbol{X}})^T \cdot \frac{\partial \bar{\boldsymbol{X}}}{\partial \boldsymbol{Q}}$$

$$\frac{\partial \bar{\boldsymbol{X}}}{\partial \boldsymbol{Q}} = \frac{\partial \bar{\boldsymbol{X}}_i}{\partial \boldsymbol{Q}} + \frac{\partial k_{i,i+1}}{\partial \boldsymbol{Q}} \cdot (\bar{\boldsymbol{X}}_{i+1} - \bar{\boldsymbol{X}}_i) + k_{i,i+1} \cdot \cdot \left(\frac{\partial \bar{\boldsymbol{X}}_{i+1}}{\partial \boldsymbol{Q}} - \frac{\partial \bar{\boldsymbol{X}}_i}{\partial \boldsymbol{Q}} \right)$$

$$\frac{\partial k_{i,i+1}}{\partial \boldsymbol{Q}} = -2\|\bar{\boldsymbol{X}}_{i+1}-\bar{\boldsymbol{X}}_i\|^{-1}\cdot\frac{\partial\|\bar{\boldsymbol{X}}_{i+1}-\bar{\boldsymbol{X}}_i\|}{\partial \boldsymbol{Q}}\cdot(\boldsymbol{S}_j^\star-\bar{\boldsymbol{X}}_i)^T\cdot$$
$$\cdot(\bar{\boldsymbol{X}}_{i+1}-\bar{\boldsymbol{X}}_i)-\|\bar{\boldsymbol{X}}_{i+1}-\bar{\boldsymbol{X}}_i\|^{-2}\cdot\frac{\partial\bar{\boldsymbol{X}}_i}{\partial \boldsymbol{Q}}^T\cdot$$
$$\cdot(\bar{\boldsymbol{X}}_{i+1}-\bar{\boldsymbol{X}}_i)+\|\bar{\boldsymbol{X}}_{i+1}-\bar{\boldsymbol{X}}_i\|^{-2}\cdot(\boldsymbol{S}_j^\star-\bar{\boldsymbol{X}}_i)^T\cdot$$
$$\cdot\left(\frac{\partial\bar{\boldsymbol{X}}_{i+1}}{\partial \boldsymbol{Q}}-\frac{\partial\bar{\boldsymbol{X}}_i}{\partial \boldsymbol{Q}}\right)$$

$$\frac{\partial\|\bar{\boldsymbol{X}}_{i+1}-\bar{\boldsymbol{X}}_i\|}{\partial \boldsymbol{Q}} = \left[(\bar{\boldsymbol{X}}_{i+1}-\bar{\boldsymbol{X}}_i)^T\cdot(\bar{\boldsymbol{X}}_{i+1}-\bar{\boldsymbol{X}}_i)\right]^{-\frac{1}{2}}\cdot$$
$$\cdot(\bar{\boldsymbol{X}}_{i+1}-\bar{\boldsymbol{X}}_i)^T\cdot\left(\frac{\partial\bar{\boldsymbol{X}}_{i+1}}{\partial \boldsymbol{Q}}-\frac{\partial\bar{\boldsymbol{X}}_i}{\partial \boldsymbol{Q}}\right)$$

where from (8) holds that

$$\frac{\partial\bar{\boldsymbol{X}}_i}{\partial \boldsymbol{Q}} = \frac{\partial\mathbf{F}(\boldsymbol{X}_k)}{\partial \boldsymbol{X}_k}\cdot\begin{bmatrix}\boldsymbol{I} & \boldsymbol{O}\\ \boldsymbol{O} & -\boldsymbol{S}(\boldsymbol{z}_k^0)\end{bmatrix}\cdot\boldsymbol{J}_k^0(\boldsymbol{Q}). \tag{16}$$

The constant k_i^1 resp. k_i^2 are the weights for the i-th extremal point distance and $[i,i+1]$-th manipulator link distance from obstacles resp. the i-th extremal point surface distance. The constants ${}^\star w_j$ are weights of the j-th obstacle.

The entire objective function results in:

$$w(\boldsymbol{Q}) = {}^1w(\boldsymbol{Q})+\sum_j\left({}^2w_j(\boldsymbol{Q})+{}^3w_j(\boldsymbol{Q})\right)$$
$$\frac{\partial w(\boldsymbol{Q})}{\partial \boldsymbol{Q}} = \sum_j\left(\frac{\partial w_j^1(\boldsymbol{Q})}{\partial \boldsymbol{Q}}+\frac{\partial w_j^3(\boldsymbol{Q})}{\partial \boldsymbol{Q}}\right)+\frac{w^2(\boldsymbol{Q})}{\partial \boldsymbol{Q}} \tag{17}$$

The objective function is then used for weighted least norm algorithm for robot body fitting around the pipe regarding obstacle avoidance. The computation of joint velocities for JOG mode[1] with respect to objective function is given as, see [10], [11]:

$$\dot{\boldsymbol{Q}} = \boldsymbol{J}^\dagger(\boldsymbol{Q})\cdot\dot{\bar{\boldsymbol{X}}}+\left(\boldsymbol{I}-\boldsymbol{J}^\dagger(\boldsymbol{Q})\cdot\boldsymbol{J}(\boldsymbol{Q})\right)\cdot\frac{\partial w(\boldsymbol{Q})}{\partial \boldsymbol{Q}} \tag{18}$$

where $\boldsymbol{J}^\dagger(\boldsymbol{Q}) = \bar{\boldsymbol{J}}^T(\boldsymbol{Q})\cdot\left(\bar{\boldsymbol{J}}(\boldsymbol{Q})\cdot\bar{\boldsymbol{J}}^T(\boldsymbol{Q})\right)^{-1}$ is a Penrose inverse of the jacobian $\bar{\boldsymbol{J}}(\boldsymbol{Q})$.

V. Command Control and Simulation

In general, the manual command control of hyper-redundant robot is impossible. The highly nonlinear kinematics, redundancy and associated non intuitive behavior totally impede the position control by operator. Therefore the motion control is based on Developed view and associated orbital level as a clear and intuitive interface between operator, weld documentation and path planner. The task of the operator is to define the weld position, obstacle envelopes, orbital level and the initial manipulator settings. Then he can command the probe speeds in the coordinates of the Developed view, typically via JOG mode. Remaining positions, speeds and acceleration of redundancy of the robot are calculated by motion planner to ensure the precise movement of the probe, avoiding the obstacles while minimizing the movement of joints. The motion planner moves the NDT probe according the operator commands or along the weld path and simultaneously tries to move each link out of obstacles envelopes and at given orbital level. The repulsive forces and attraction to orbital level can be easily tuned by operator using the constants k_i. Moreover this behavior can be tuned for each joint-link independently.

[1]During JOGging, the operator can move the robot in the required direction by pushing the JOG keys on the teach pendant. We suppose only velocities (without position compensation). It is sufficient for robot JOG mode.

Simulation results

The inverse kinematic algorithm given by (18) with respect to the objective function (17) was demonstrated on the virtual simulation model of 13 DoF manipulator commanded by end-effector speed represented in DV coordinates (6). The initial position of the manipulator (without optimization) is depicted in Fig. 8 and the resulting position of the manipulator after its internal optimal reconfiguration is depicted in Fig. 9. The screen shots of the manipulator motion enforced by the JOG in the $\boldsymbol{l}$, $\boldsymbol{z}$ and $\boldsymbol{\alpha}$ directions are depicted in $l-z$ plane in Fig. 10 (circular obstacle avoidance) and in $x-y$ plane in Fig. 11 (orbital level hovering).

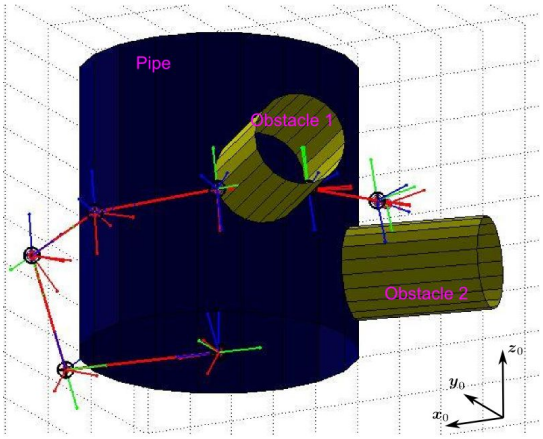

Fig. 8. Initial position of the manipulator (SimMechanics model).

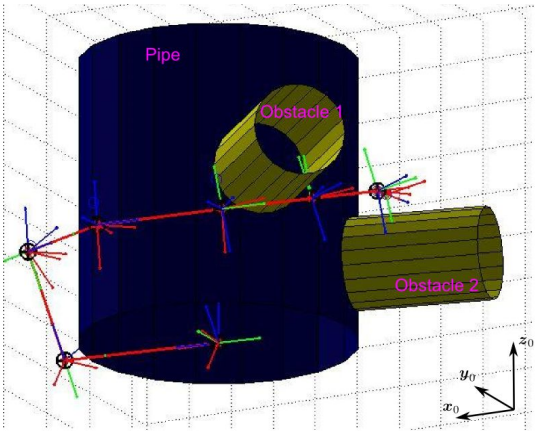

Fig. 9. Resulting position of the manipulator (SimMechanics model).

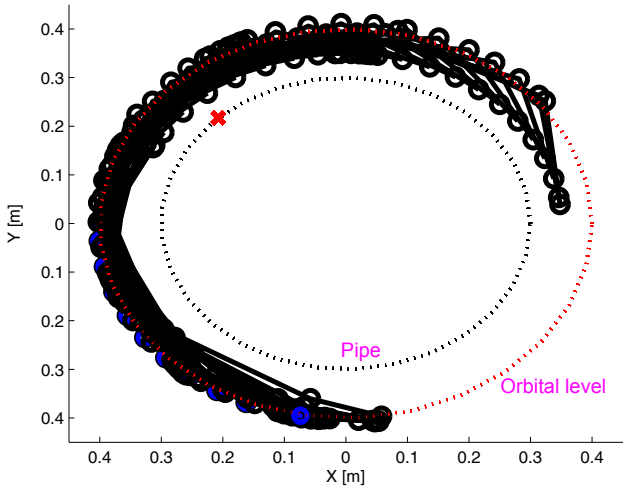

Fig. 11. Optimal motion of the proposed manipulator during the coordinated JOG (orbital level hovering).

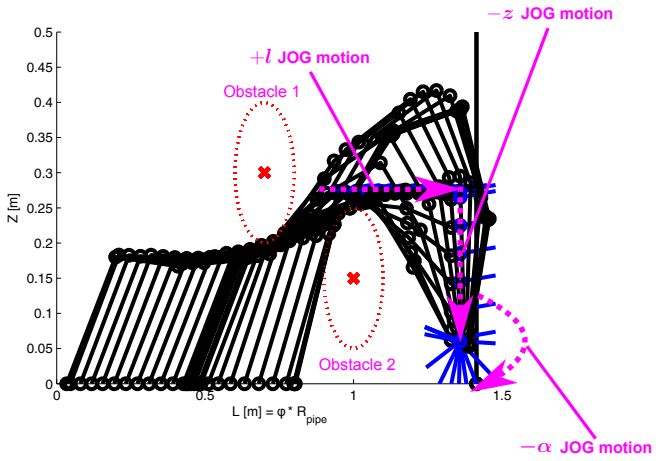

Fig. 10. Optimal motion of the proposed manipulator during the coordinated JOG (circular obstacle avoidance).

VI. Conclusion

The paper was devoted to path planning method of hyper-redundant NDT manipulator. According to given demands on NDT inspection process, it is very useful to restrict the path planner to work in Developed view of given cylindrical work space. The transformation from robot joint space to Developed view and back was described and used for path planning and obstacle avoidance. It helps to simplify the computational process and understand the robot complex behavior during motion in constrained environment.

The main features can be summarized as follows:

- An intuitive representation of the trajectory planning (JOG) in the Developed view - only four, naturaly represented coordinates.
- The common obstacles representation in the Developed view (orbital level, perpendicular pipe inlet envelope) which corresponds to the standard pipeline system and appropriate welds documentation in power plants.
- Implemented JOG function can be easily modified to optimal joint coordinates computation from prescribed end-effector trajectory (automated weld testing in restricted areas).

Acknowledgment

This work was supported by the project LO1506 of the Czech Ministry of Education, Youth and Sports, and the Technology Agency of the Czech Republic under Grant TF02000041.

References

[1] P. Liljebäck, K. Y. Pettersen, O. Stavdahl, and J. T. Gravdahl. Snake Robots: Modelling, Mechatronics, and Control. Springer Publishing Company, Incorporated, 2012.

[2] R. V. Agthoven, F Dijkstra and J. d. Raad, A lifetime of meeting challenges through innovative solutions at Applus RTD, 2013.

[3] R. L. Halton, H. Choset, Generating gaits for snake robots: annealed chain fitting and keyframe wave extraction, Autonomous Robots, 2010.

[4] W.A.Wolovich and H.Elliott, A computational technique for inverse kinematics, in Proc. 23rd IEEE Conf. on Decision and Control (Las Vegas, NV. Dec. 1984).

[5] L. Sciavicco and B. Siciliano, A solution algorithm to the inverse kinematic problem for redundant manipulators, IEEE J. Robot. Autom. ,vol.4, no. 4, pp. 403410, Aug. 1988.

[6] B. Siciliano, Kinematic control of redundant robot manipulators: A Tutorial, J. Intell. Robot. Syst., vol. 3, pp. 201212, 1990.

[7] M. Švejda, "New robotic architecture for NDT applications." IFAC Proceedings Volumes 47.3, 2014, pp. 11761-11766.

[8] L. Bláha, "Design of a compact 2-DOF joint with belt driven actuators," 2017 IEEE 4th International Conference on Soft Computing and Machine Intelligence (ISCMI), Mauritius, Mauritius, 2017, pp. 198-202. doi: 10.1109/ISCMI.2017.8279626

[9] Denavit, J., Hartenberg, R. S., A kinematic notation for lower-pair mechanisms based on matrices, Trans. of the ASME. Journal of Applied Mechanics, 1955, vol. 22, pp. 215-221.

[10] Siciliano, B., Kinematic control of redundant robot manipulators: A tutorial Journal of Intelligent and Robotic Systems, Kluwer Academic Publishers, 1990, 3, 201-212.

[11] Sciavicco, L., Siciliano, B., Modelling and Control of Robot Manipulators, Springer London, 2000.